The Astrophysical Journal, 974:241 (15pp), 2024 October 20 https://doi.org/10.3847/1538-4357/ad64d3

Radio Afterglows from Tidal Disruption Events: An Unbiased Sample from ASKAP RACS

Akash Anumarlapudi[1], Dougal Dobie[2,3,4], David L. Kaplan[1], Tara Murphy[3,4], Assaf Horesh[5], Emil Lenc[6], Laura Driessen[4], Stefan W. Duchesne[7], Hannah Dykaar[8,9], B. M. Gaensler[8,9,10], Timothy J. Galvin[7,11], Joe Grundy[7,11], George Heald[7], Aidan W. Hotan[7], Minh Huynh[7], James K. Leung[5,8], David McConnell[6], Vanessa A. Moss[4,6], Joshua Pritchard[3,4,6], Wasim Raja[6], Kovi Rose[4,6], Gregory Sivakoff[12], Yuanming Wang[2,3], Ziteng Wang[11], Mark H. Wieringa[6], and Matthew T. Whiting[6]
[1] Department of Physics, University of Wisconsin-Milwaukee, P.O. Box 413, Milwaukee, WI 53201, USA; aakash@uwm.edu
[2] Centre for Astrophysics and Supercomputing, Swinburne University of Technology, Hawthorn, VIC 3122, Australia
[3] ARC Centre of Excellence for Gravitational Wave Discovery (OzGrav), Hawthorn, VIC, Australia
[4] Sydney Institute for Astronomy, School of Physics, University of Sydney, NSW 2006, Australia
[5] Racah Institute of Physics, The Hebrew University of Jerusalem, Jerusalem, 91904, Israel
[6] CSIRO Space and Astronomy, P.O. Box 76, Epping, NSW 1710, Australia
[7] CSIRO Space and Astronomy, P.O. Box 1130, Bentley, WA 6102, Australia
[8] Dunlap Institute for Astronomy and Astrophysics, University of Toronto, 50 St. George St., Toronto, ON M5S 3H4, Canada
[9] David A. Dunlap Department of Astronomy and Astrophysics, University of Toronto, 50 St. George St., Toronto, ON M5S 3H4, Canada
[10] Department of Astronomy and Astrophysics, University of California Santa Cruz, 1156 High Street, Santa Cruz, CA 95064, USA
[11] International Centre for Radio Astronomy Research—Curtin University, 1 Turner Avenue, Bentley, WA 6102, Australia
[12] Department of Physics, University of Alberta, CCIS 4-181, Edmonton, AB T6G 2E1, Canada
Received 2024 March 1; revised 2024 July 12; accepted 2024 July 15; published 2024 October 15

Abstract

Late-time (∼a year) radio follow-up of optically discovered tidal disruption events (TDEs) is increasingly resulting in detections at radio wavelengths, and there is growing evidence for this late-time radio activity to be common to the broad class of subrelativistic TDEs. Detailed studies of some of these TDEs at radio wavelengths are also challenging the existing models for radio emission. Using all-sky multiepoch data from the Australian Square Kilometre Array Pathfinder (ASKAP), taken as a part of the Rapid ASKAP Continuum Survey (RACS), we searched for radio counterparts to a sample of optically discovered TDEs. We detected late-time emission at RACS frequencies (742–1032 MHz) in five TDEs, reporting the independent discovery of radio emission from TDE AT 2019ahk and extending the time baseline out to almost 3000 days for some events. Overall, we find that at least 22^{+15}_{-11}% of the population of optically discovered TDEs has detectable radio emission in the RACS survey, while also noting that the true fraction can be higher given the limited cadence (two epochs separated by ∼3 yr) of the survey. Finally, we project that the ongoing higher-cadence (∼2 months) ASKAP Variable and Slow Transients survey can detect ∼20 TDEs in its operational span (4 yr), given the current rate from optical surveys.

Unified Astronomy Thesaurus concepts: Radio transient sources (2008); Tidal disruption (1696); Extragalactic radio sources (508); Radio continuum emission (1340); Radio sources (1358)

Materials only available in the online version of record: machine-readable tables

1. Introduction

The discovery of tidal disruption events (TDEs; Rees 1988) thus far was initially dominated by X-ray surveys (Halpern et al. 2004) and then by optical/ultraviolet (O/UV) surveys in more recent times (van Velzen et al. 2021; Hammerstein et al. 2023; Yao et al. 2023). At O/UV wavelengths, emission from TDEs has a characteristic blue continuum with hydrogen and/or helium emission lines and can be accurately modeled as a blackbody with temperatures peaking near UV wavelengths (Gezari 2021).[13] Radio emission from TDEs, expected from the interaction of nascent jets or outflows, was initially detected only in a handful of TDEs, and this initial sample was dominated by TDEs that were discovered at higher energies. It was estimated by Alexander et al. (2020) that not all TDEs result in radio detections, with only ∼20% of them being radio-bright. The distribution of radio luminosities from this initial crop of TDEs indicated a dichotomy at radio wavelengths where the luminosity differed by 2–3 orders of magnitude (Alexander et al. 2020). The more luminous events resulted from relativistic jetted TDEs in which the radio luminosity exceeded 10^{40} erg s^{-1}, while the less luminous events were from TDEs with subrelativistic outflows where the isotropic radio luminosity was around 10^{38} erg s^{-1} (Zauderer et al. 2011; Alexander et al. 2016, 2020).

Shock-accelerated relativistic electrons produce radio emission from TDEs via the synchrotron mechanism (Alexander et al. 2020). This can be due to external shocks driven by jets/outflows or unbound stellar debris into the circumnuclear medium (CNM; Zauderer et al. 2011; Alexander et al. 2016; Krolik et al. 2016) or due to internal shocks within the jet (Pasham & van Velzen 2018). By modeling the spectral and temporal evolution of the emission, one can estimate the jet/outflow properties, particularly the velocity of the ejecta, their launch time relative to the optical flare, and the energy injected

[13] This is true for Sun-like stars. In general, the spectral signature depends on the composition of the disrupted star.

Table 1
Survey Details of All the Different Surveys Used as a Part of this Article

Survey	RACS-low (Epoch 1)	RACS-low (Epoch 2)	RACS-mid	RACS-high	VLASS
Center frequency (MHz)	887.5	887.5	1367.5	1655.5	3000
Bandwidth (MHz)	288	288	144	200	2000
Sky coverage	$-90^\circ < \delta < +41^\circ$	$-90^\circ < \delta < +51^\circ$	$-90^\circ < \delta < +49^\circ$	$-90^\circ < \delta < +48^\circ$	$-40^\circ < \delta < +90^\circ$
Integration time	15 minutes	15 minutes	15 minutes	15 minutes	5 s
Median noise (mJy beam^{-1})	0.25	0.19	0.20	0.19	0.12
Angular resolution	$\sim 15''$	$\sim 15''$	$\sim 10''$	$\sim 8''$	$2.''5$
Observations	~2019 March	~2022 March	~2021 January	~2021 December	…[a]
Instrument	ASKAP	ASKAP	ASKAP	ASKAP	VLA
Reference	McConnell et al. (2020)	In preparation	Duchesne et al. (2023)	In preparation	Lacy et al. (2020)

Note.
[a] The first two epochs of VLASS were completed roughly in 2019 and 2021, and the third observing run is currently ongoing.

into the CNM (Granot & Sari 2002; Barniol Duran et al. 2013; Matsumoto & Piran 2023). Continuous monitoring of events in which early-time (a few days to weeks after the optical flare) radio emission was detected, such as Swift J1644+57 (Zauderer et al. 2011) and ASASSN-14li (Alexander et al. 2016), demonstrated that the radio emission can be very long-lived, until years after the disruption.

However, there are TDEs like ASASSN-15oi and AT 2018hyz in which early-time radio observations resulted in null detections, yet continued monitoring of these events until late time (a few months to years after the optical flare) resulted in radio detections (Horesh et al. 2021; Cendes et al. 2022). This can be due either to a delay in the ejection of the outflow (Cendes et al. 2022) or to the viewing effects of an off-axis observer looking at a relativistic jet (Matsumoto & Piran 2023; Sfaradi et al. 2024). In addition, Horesh et al. (2021) found a radio rebrightening in ASASSN-15oi, ~4 yr after the initial optical discovery. Horesh et al. (2021) and Cendes et al. (2022) showed that the radio light curve in both these events showed a rise/decline that is steeper than any of the current predictions. More recently, studying late-time radio activity in TDEs using a sample of 23 TDEs, Cendes et al. (2024) showed that the launch of the outflow can be delayed, by as much as ~700 days, which raises the question of whether the phenomenon of delayed ejection is common in TDEs and whether the current models are adequate for describing the observed emission in TDEs like these.

While large samples of TDEs are coming from ongoing optical surveys (van Velzen et al. 2020; Gezari 2021; Yao et al. 2023), the discovery space is expanding. Recent studies such as those of Jiang et al. (2016), van Velzen et al. (2016, 2021), Jiang et al. (2021a, 2021b), and Masterson et al. (2024) have discovered TDEs at infrared (IR) wavelengths using dust echoes from TDEs. Using the first two epochs of the Very Large Array Sky Survey (VLASS; Lacy et al. 2020), Somalwar et al. (2023) produced an independent sample of six radio TDEs that are optically bright. A few TDEs in this sample showed lower blackbody temperatures ($T_{\rm bb}$) and luminosities ($L_{\rm bb}$) than the optically discovered TDEs, indicating TDEs occurring in dust-obscured environments and adding to the sample of radio-first TDE discoveries (Anderson et al. 2020; Ravi et al. 2022). Such independent TDE discoveries from highly dust-obscured regions at radio/IR wavelengths can help constrain the true rate of TDEs and resolve the tension between the observed rate and the rate expected from theoretical predictions (Alexander et al. 2020; Gezari 2021; Yao et al. 2023). Using the first 3 yr of data from the Zwicky Transient Facility (ZTF; Bellm et al. 2019), Yao et al. (2023) estimated a volumetric rate of $3.1^{+0.6}_{-1.0} \times 10^{-7}\,{\rm Mpc^{-3}\,yr^{-1}}$ TDEs ($L_{\rm bb} > 10^{43}\,{\rm erg\,s^{-1}}$). Comparing the rate of thermal TDEs to Swift J1644-like X-ray events (Alexander et al. 2020) and AT 2020cmc-like optical events (Andreoni et al. 2022), the relative rate of jetted TDEs is estimated to be less than 1% of that of thermal TDEs. This implies that the observed rate of thermal plus jetted TDEs is still lower than the current theoretical prediction by an order of magnitude (Gezari 2021).

All-sky radio surveys can be an extremely useful resource in discovering radio afterglows serendipitously. However, multi-epoch data can be crucial to separate emission related to the TDE from emission from any active galactic nucleus (AGN) that may be present. In particular, high-cadence surveys like the Australian SKA Pathfinder Variable and Slow Transients survey (ASKAP VAST. Murphy et al. 2013, 2021) can be very fruitful in getting a well-sampled light curve for a larger sample of TDEs where dedicated follow-up of every individual event may not be possible/practical (see, e.g., Leung et al. 2023, for a serendipitous discovery of an off-axis TDE afterglow candidate).[14] Motivated by this, we used the data from the Rapid ASKAP Continuum Survey (RACS; McConnell et al. 2020; Hale et al. 2021), a multiepoch all-sky survey (see Table 1 for survey details) to search for radio emission from TDEs discovered at higher energies (O/UV/X-ray). We then studied the prospects of finding radio TDEs in the VAST survey by projecting the rates estimated from the fraction of TDEs that are radio-bright in the RACS survey.

An alternative approach to discovering TDEs by modeling the evolution of the radio light curve using existing models (e.g., Nakar & Piran 2011) is used by Dykaar et al. (2024) to independently discover TDE candidates at radio wavelengths. Our approach is different from their untargeted and model-dependent search, yet complementary since we find afterglows from TDEs such as ASASSN-15oi, AT 2018hyz, etc., in which the observed radio emission cannot be easily explained by the existing models. Unlike dedicated follow-up campaigns that extensively monitor a given sample of TDEs (Cendes et al. 2024; Somalwar et al. 2023), our approach is different, in that we study the prospects of discovering TDEs serendipitously in all-sky surveys, and hence our data are sparser. We focus instead on the nature of the TDEs we detect at lower observing frequencies, their rates, and the implications and expectations for the VAST survey.

[14] VAST has a cadence of 2 weeks–2 months depending on the sky position.

Our article is structured as follows. In Section 2, we detail our observations, surveys used in this study, and our data reduction methods. In Section 2.4, we discuss our sample selection technique. We present our detections in Section 3 and describe the properties of the individual candidates in Sections 3.1 through 3.6. Finally, we discuss the implications of our detections in Section 4 and projections for future surveys like VAST in Section 4.2, before concluding in Section 5.

Throughout this work, we use the Planck Collaboration et al. (2020) model of cosmology, with $H_0 = 67.4\ \mathrm{km\ s^{-1}\ Mpc^{-1}}$.

2. Observations and Data Analysis

2.1. Rapid ASKAP Continuum Survey

The primary data set used in this work comes from all-sky 887.5 MHz radio observations taken as a part of RACS—RACS-low. RACS-low has been conducted at two separate epochs thus far, separated by ∼3 yr. In addition, RACS has also been conducted at two other frequencies, as single-epoch (so far) surveys—RACS-mid (1367 MHz; Duchesne et al. 2023) and RACS-high (1655 MHz; in preparation), data from which we have used to study the behavior of the TDEs that we detected in RACS-low. Details of each of these surveys are provided in Table 1.

Observations for all of the RACS surveys were carried out between 2019 March and 2022 April. Data were processed using standard techniques recommended for ASKAP data (Hotan et al. 2021) and using the ASKAPsoft package (Guzman et al. 2019) to generate both the images and the noise maps. A more detailed description of reduction techniques is provided by McConnell et al. (2020). In this paper, we only used the total intensity (Stokes *I*) maps.

2.2. Variable and Slow Transients Survey

VAST (Murphy et al. 2013, 2021) is a radio survey that will image almost one-quarter of the entire sky repeatedly for 4 yr. VAST is divided between the Galactic sky and extragalactic sky, with the Galactic sky being observed with a cadence of roughly 2 weeks and the extragalactic sky with a cadence of roughly 2 months. VAST pilot surveys (Murphy et al. 2021) were carried out in-between the two RACS-low epochs, and the main VAST survey began its operation in 2022 December.[15] For the TDEs that we detected in the RACS-low data set, we augmented the RACS data with data from the VAST survey, if the transient falls inside the VAST footprint. The survey parameters of VAST are similar to those of the RACS-low survey (see Table 1), except for a 12 minutes integration time per field in VAST compared to a 15 minutes observation in RACS. A more detailed description of the pilot and full surveys is provided by Murphy et al. (2013, 2021), Leung et al. (2023), and Pritchard et al. (2024).

2.3. VLA Sky Survey

In addition to the RACS and VAST survey data, we also made use of the VLASS (Lacy et al. 2020). VLASS is an all-sky survey spanning 2–4 GHz and plans to scan the entire sky at three different epochs with a cadence of roughly 32 months between the epochs.[16] The first two epochs have been completed and the third is underway. For the TDEs detected in RACS-low data, we used the VLASS quick-look images (Lacy et al. 2020) to measure the flux density at 3 GHz.[17]

2.4. Search Methodology

We selected all the TDEs from the transient network server (TNS)[18] that were spectroscopically classified as TDEs, as well as those that were optically discovered in all-sky surveys such as the ZTF and All-Sky Automated Survey for Supernovae (ASAS-SN; Shappee et al. 2014),[19] which resulted in 63 events (Auchettl et al. 2017; Hammerstein et al. 2023; Yao et al. 2023). We then discarded 13 events that are outside the RACS-low epoch 1 footprint, as well as those events where the optical discovery occurred after RACS-low epoch 2, leaving 43 events in our sample. We examined the RACS-low total intensity (Stokes *I*) sky maps to look for radio emission at the TDE positions. Radio emission in TDEs can be observable years after the initial disruption (see Alexander et al. 2020; Cendes et al. 2022, 2024; Sfaradi et al. 2024), and hence we restricted our cross-match to spatial coincidence, relaxing any constraint on the temporal coincidence as long as the TDE was discovered before the second RACS-low epoch.[20] The positional accuracy for the ASKAP data is 2.″5, and hence we used twice this as our search radius, 5″, when astrometrically cross-matching the TDEs.[21] This resulted in 11 TDEs for which we detected coincident radio emission in RACS-low. However, only five of these events showed significant variability in their light curve between the two RACS-low epochs. The remaining six events did not show any significant evolution between the RACS-low epochs, which made it difficult to rule out underlying emission from the host galaxy/host AGN (see Section 3.6 for more details).

In the five TDEs with coincident variable radio emission, the emission lasted some years after the initial optical outburst, with the longest-lived radio TDE lasting ∼8 yr. Our detections add to the sample of TDEs reported by Cendes et al. (2024), where late-time radio emission is seen. However, only one TDE (AT 2018hyz) is common to our sample and Cendes et al. (2024). Table A1 gives the flux density measurements for all these events. For all the TDEs that are in the RACS footprint but resulted in nondetections we provide upper limits (3σ) on the radio flux density and radio luminosity in Table A2.

3. Individual Tidal Disruption Events

Given the nature of this study, our light curves are sparser than in dedicated campaigns like those of Goodwin et al. (2022b) or Cendes et al. (2022, 2024). We therefore make simplifying assumptions about the spectral and temporal properties of the observed emission to estimate the source properties. We modeled the late-time radio spectrum as a broken power law with the break frequency corresponding to the synchrotron self-absorption (SSA) frequency ($\nu_{\rm ssa}$), but adapted from Granot & Sari (2002) to join the power laws smoothly (see case 2 of Figure 1 of Granot & Sari 2002). We

[15] https://www.vast-survey.org/Survey/
[16] North of −40° decl.
[17] https://archive-new.nrao.edu/vlass/quicklook/
[18] https://www.wis-tns.org/
[19] https://www.astronomy.ohio-state.edu/asassn/
[20] The radio emission can persist for years after the optical flare in a few TDEs (such as Swift J1644; Zauderer et al. 2011), but is only observable at late times in a few others (such as ASASSN-15oi; Horesh et al. 2021).
[21] This is including the systematic component of the offset (see McConnell et al. 2020).

modeled the temporal evolution of the light curve using Chevalier (1998): a rising power law when the emission is optically thick, joined smoothly by a declining power law when the emission becomes optically thin.

To infer source parameters we assume that the energy stored in magnetic fields is similar to the energy of the relativistic electrons, (*equipartition*; Pacholczyk 1970). Since the timescale of our radio detections is a year or more, we assume—unless we see evidence for on-axis jets (radio luminosity consistent with Swift J1644 or AT 2020cmc-like events) or off-axis relativistic jets (characterized by a steep rise)—that the bulk Lorentz factor is close to 1 (Newtonian case). We assume that roughly 10% of the energy in heavy particles is used to accelerate the electrons to relativistic speeds ($\epsilon_e \approx 0.1$). Assuming a power-law seed electron energy distribution $N(E)dE = AE^{-p}$, with p being the index, we infer the emission radius ($R_{\rm eq}$) and the total equipartition energy following Barniol Duran et al. (2013).[22] We caution that the outflow geometry of sub/nonrelativistic outflows can be quasi-spherical or asymmetrical, in which the filling factors can differ, but as noted by Pacholczyk (1970), the estimated source properties are relatively insensitive to these. Hence, in this work, we assume that the geometry is nearly spherical. Further, we assume that the observed radio emission arises from a thin shell of expanding outflow (of width $\approx 0.1R$, where R is the radius, e.g., Alexander et al. 2016) and is spherically symmetric. For such cases, the areal and volume filling factors, f_A and f_V (see Barniol Duran et al. 2013), are 1 and 0.36 respectively.

3.1. ASASSN-15oi

After an initial nondetection at radio wavelengths (up to ∼6 months), Horesh et al. (2021) reported the discovery of a radio counterpart to ASASSN-15oi (Holoien et al. 2016) that rose steeply ($\sim t^4$). This was followed by a steep fall (steeper than t^{-3}) that became shallower at late times (see Figure 1). Horesh et al. (2021) noted that such a steep rise and fall could not be explained by a standard forward shock and CNM interaction model. Horesh et al. (2021) also reported a very late-time rebrightening (∼1000 days later) in the VLASS epoch 1 data.

We detected very late-time rebrightening in RACS-low data, and the light curve continued to rise (roughly as $\sim t^2$) and peaked ∼2500 days after the optical flare (see Figure 1). This very late-time rebrightening was replicated in the RACS-mid and RACS-high data as well. VAST observations for this transient revealed that the emission started to decline steeply ($\sim t^{-3}$) following the peak. This very late-time decline is similar to the behavior that Horesh et al. (2021) reported following the initial radio peak. A. Horesh et al. (2021) point out, the changes in various rates of decline of emission could point to changes in the CNM density profile or a structured jet. However, it is difficult to reconcile such steep rises and falls with the existing afterglow models.

Using the second epoch of VLASS observations, we find that the 3 GHz light curve is declining, roughly following a t^{-1} decline (see Figure 1). This is in contrast to the rising 887.5 MHz light curve during the same period, which suggests that the emission at 3 GHz was optically thin during this period

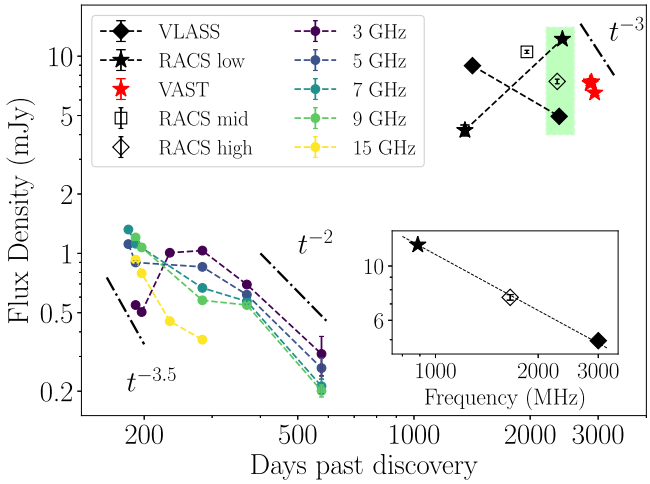

Figure 1. Light curve of the TDE ASASSN-15oi using RACS, VLASS, and archival data. In all the figures in this article, RACS-low data are shown as black stars, RACS-mid as open black squares, RACS-high as open black diamonds, and VLASS data as filled black diamonds. RACS data combined with the data from the VAST full survey, shown as red stars, reveal the rise and decline of the 888 MHz light curve. Shown as multicolored dots is the archival light curve, from 3 to 15 GHz, adapted from Horesh et al. (2021). The green stripe shows the data used to estimate the electron distribution index. The inset shows this spectrum, and the dashed line in the inset shows the best-fit power law to these data (see text for more details). Shown as dashed–dotted lines are the visual guides for different power-law declines.

and that at 887.5 MHz was optically thick. This can be explained by the peak frequency gradually transitioning to lower frequencies at late times, a trend that is expected and was also observed by Horesh et al. (2021) during the initial radio observations. This is also consistent with our 887.5 MHz observations, which revealed a turnover indicative of emission transitioning from optically thick to thin at >3000 days.

The RACS-high, VLASS epoch 2, and the RACS-low epoch 2 data are separated by ∼75 days, and under the assumption that the spectral evolution during this time frame is minimal (given the active cycle of >4 yr), we found that the spectrum at this epoch (∼2400 days after the event) is well fit by a power law (with the spectral index, $\alpha = -0.75 \pm 0.2$, where $S_\nu \propto \nu^\alpha$). We assumed that the self-absorption frequency is closer to the RACS observing frequency (887.5 MHz),[23] without attempting a physical model for the origin of this, and estimate the electron distribution index $p = 2.5 \pm 0.2$.[24] Given the peak frequency $\nu_{\rm p} \approx 887.5$ MHz, the peak flux density $F_{\nu,{\rm p}} = 12.2$ mJy, and $p = 2.5$, we derive lower limits of $R_{\rm eq} \approx 6 \times 10^{17}$ cm on the emission radius and $E_{\rm eq} \approx 1 \times 10^{50}$ erg on the total energy.

3.2. AT 2019ahk/ASASSN-19bt

AT 2019ahk was discovered as an optical transient by Holoien et al. (2019). We report an independent radio discovery of this event in RACS data at all three frequencies (see Figure 2), where we saw a rising transient over 3 yr. Christy et al. (2024) report archival radio detection of AT 2019ahk roughly 4 yr before the disruption and estimate underlying host galaxy emission to follow $F_{\nu,{\rm host}} =$

[22] Since the peak frequency corresponds to $\nu_{\rm ssa}$, we correct the total equipartition energy by accounting for the radiation emitted at ν_m.

[23] The radio emission being optically thick at 887.5 MHz at this time (which continues until ∼2800 days after the disruption) and thin at 3 GHz partially supports this assumption.

[24] Horesh et al. (2021) found that the initial radio spectrum showed large deviation from the SSA spectrum in the self-absorbed part, but might be consistent with free–free absorption.

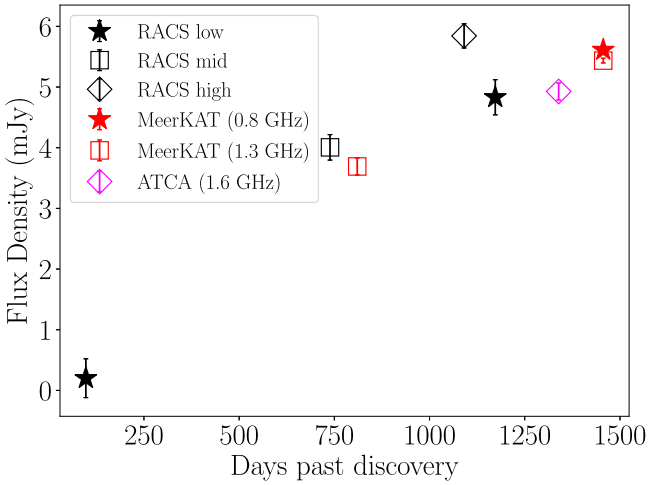

Figure 2. Light curve of the TDE AT 2019ahk confirming the late-time rise of the radio light curve at all the RACS observing frequencies. Also shown are the contemporary data at 1.3 and 1.6 GHz adapted from Christy et al. (2024), showing the continued rise of the 0.8–0.9 GHz light curve and the turnover of the 1.6 GHz light curve. This source is too far south for VLASS.

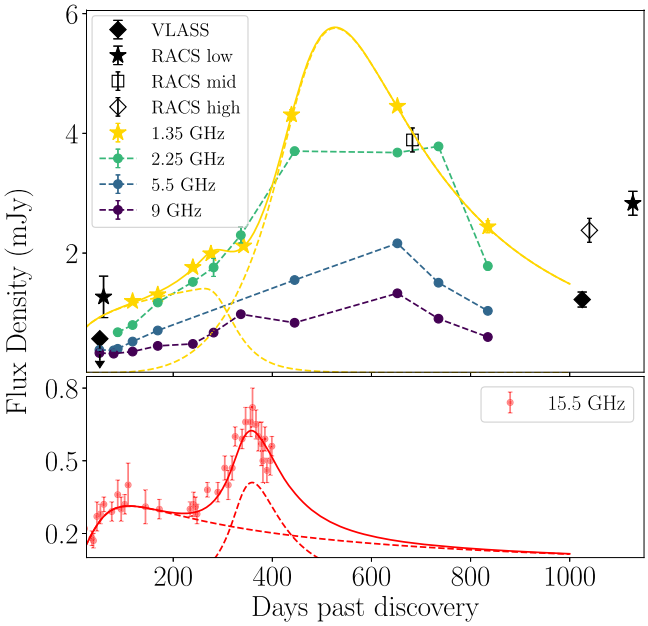

Figure 3. Top panel: the light curve using archival data (from Goodwin et al. 2022b; Sfaradi et al. 2022) is shown at four different frequencies (1.35, 2.25, 5.5, and 9 GHz). The yellow curve is the best-fit model for the 1.4 GHz data (see text for the model), with the dashed lines representing the individual components and the solid line indicating their sum. Bottom panel: 15.5 GHz light curve for reference using the data from Sfaradi et al. (2022). The red curve is the two-component model proposed by Sfaradi et al. (2022), with the dashed line representing the individual components and the solid line, their sum.

0.439 $(\nu/2.1\ \mathrm{GHz})^{-1}$ mJy. Combining the RACS data with contemporaneous data from Christy et al. (2024), we see that the 0.8–0.9 GHz light curve is still rising ≈1500 days after the event, but the 1.6 GHz light curve started to decline. This hints that emission at 1.6 GHz has transitioned to an optically thin regime, but emission at lower frequencies is still optically thick. Hence, the SSA frequency is very close to the RACS-high frequency at ≈1100 days, consistent with the peak frequency estimated by Christy et al. (2024). Using $p \approx 2.7$, using the existing literature (e.g., Cendes et al. 2022, 2024; Goodwin et al. 2022b), and also consistent with Christy et al. (2024), we estimate the equipartition emission radius for $\nu_{\rm p} = 1.655$ GHz, $F_{\nu,{\rm p}} = 6.4$ mJy to be $\approx 1 \times 10^{17}$ cm and the total energy to be $\approx 7 \times 10^{48}$ erg at $\delta t = 1100$ days.

3.3. AT 2019azh

Using multifrequency observations of multiple epochs, Goodwin et al. (2022b) modeled the radio spectrum of AT 2019azh to find a free expansion of the ejecta that showed signs of deceleration after ∼450 days of the disruption. Sfaradi et al. (2022), on the other hand, modeled the 15.5 GHz light curve and found evidence for two emission components (see Figure 3), which led the authors to propose a state transition similar to the ones observed in X-ray binaries.

We found this TDE in the RACS-low data as a slowly rising source, increasing by a factor of ∼2 between the two epochs. We also detected this source in the RACS-mid and RACS-high data sets. Using the RACS-mid data and the data from Goodwin et al. (2022b), we modeled the 1.4 GHz light curve reasonably well by a two-component model similar to Sfaradi et al. (2022). Figure 3 shows the full light curve for this event where the similarity can be seen between the shapes of the 15.5 and 1.4 GHz light curves, although the rise and fall times at these frequencies are different. At 1.4 GHz, the two components rose to a peak at ∼300 and 520 days respectively, slower than the 15.5 GHz light curve, which took 130 and 360 days to rise. This is broadly consistent with the underlying model (Chevalier 1998) where the emission at different frequencies is self-similar but the emission at lower frequencies has longer rise times.

However, the very late-time ($\gtrsim$3 yr) relative behavior between the RACS-mid and the RACS-high data is puzzling. Goodwin et al. (2022b) noted that the peak frequency at late times was <1 GHz, which meant that the spectrum above this should be a declining one. But the observed flux density in RACS-high is higher than the model-predicted flux density in RACS-mid by a factor that is roughly consistent with the SSA mechanism (where $S_\nu \propto \nu^{5/2}$). This might be indicative of the peak frequency increasing to higher frequencies at late times, something that Cendes et al. (2022) observed in another event, AT 2018hyz, indicative of late-time source activity. The RACS-low second-epoch detection postdates this, but the lack of continued coverage through very late times makes it difficult to distinguish whether this is consistent with the initial decline or is a signature of very late-time rebrightening, as hinted by the RACS-high data.

The RACS-high and VLASS observations are separated by ≈14 days; under the assumptions that (i) this interval is much shorter than the evolutionary timescale of the radio emission, and (ii) the peak frequency rose, but to a value lower than the observing frequency of RACS-high, we estimated the electron distribution index to be $p = 3.2 \pm 0.4$ (at $\Delta t = 1030$ days), consistent with the electron distribution of Goodwin et al. (2022b) at late times (849 days). This seems to hint that the emission we see at very late times might still be coming from the same family of electrons.

3.4. AT 2018hyz

AT 2018hyz was first detected at radio wavelengths ∼2.5 yr after the optical outburst (Horesh et al. 2022), and showed an unusually steep rise ($\sim t^{4-6}$) at most of the observed frequencies (1.3–19 GHz) (Cendes et al. 2022; Sfaradi et al. 2024).

Cendes et al. (2022) noted that the light curve at lower frequencies ($\lesssim$3 GHz) began to decline (see Figure 4) at the end of their observing campaign ($\sim$1250 days past optical outburst). Modeling the spectrum at multiple epochs, Cendes et al. (2022) also found that the peak frequency increased roughly from 1.5 to 3 GHz at late times. However, following the off-axis jet model proposed by Matsumoto & Piran (2023), Sfaradi et al. (2024) showed that the observed radio emission in AT 2018hyz is also consistent with late-time emission from a narrow jet ($\sim$7°) as viewed by an off-axis observer ($\sim$42°).

Upon finding this source in RACS-low data, we looked at the detailed VAST light curve and found no discernible radio emission until late times and a very steep rise at late times ($\sim t^4$ rise; see Figure 4), both of which were consistent with Cendes et al. (2022) and Sfaradi et al. (2024). We also found that the 887.5 MHz emission continued to rise until our final observation ($\Delta t = 1700$ days).[25] However, given the steep rise of this particular transient and the gap between RACS-low epoch 2 and the VAST full survey data, we cannot rule out a decline seen by Cendes et al. (2022) at frequencies below 3 GHz, followed by a rebrightening at 887.5 MHz instead of a single brightening episode.

We then investigated the sudden jump in the peak frequency from 1.5 GHz to 3 GHz reported by Cendes et al. (2022; see their Figure 3 and Section 4.1). At day 1251, Cendes et al. (2022) found that the peak frequency is 1.5 GHz but the data used in this fit were all at frequencies >1.12 GHz, where the self-absorbed part of the spectrum might not have been well captured. Combining the 887.5 MHz RACS data from day 1263 with the data from day 1251, we found that the peak frequency rose to 1.9 GHz as opposed to 1.5 GHz. At this epoch, we also find that the absorption part of the spectrum is more or less consistent ($S_\nu \sim \nu^{2.7}$) with what is expected from the SSA mechanism ($S_\nu \propto \nu^{5/2}$). This rise in the peak frequency to roughly 3 GHz at day 1282 might be explained by this gradual increase in the peak frequency rather than a sudden shift, something similar to what we found in AT 2019azh (see Section 3.3).

Using the latest epoch of VLASS data, we found that the 3 GHz emission also rose from an early nondetection as t^4 (see Figure 4), consistent with the RACS/VAST data, to a remarkably bright 16.5 mJy. This is consistent with the very late-time brightening of this transient in radio.

3.5. AT 2019qiz

AT 2019qiz (Siebert et al. 2019; Nicholl et al. 2020; Hung et al. 2021; Patra et al. 2022) has received comparatively very little follow-up at radio wavelengths, with O'Brien et al. (2019a, 2019b) presenting the initial radio detections that indicated a rising transient at multiple frequencies but no robust analysis presented (see Figure 5).

We found this transient in RACS-low data brightening from a nondetection in epoch 1 to a flux density level of $\sim$1 mJy in the second epoch of RACS-low, consistent with RACS-mid and RACS-high. This suggests that this source might be very slowly evolving or that it may be steadily emitting at higher flux density levels. The VAST full survey data resulted in a nondetection, which indicated that the variation in flux density

[25] Using the data from our latest observation at 1757 days, we find a hint of a turnover in the 887.5 MHz light curve, but we need additional data to robustly confirm this.

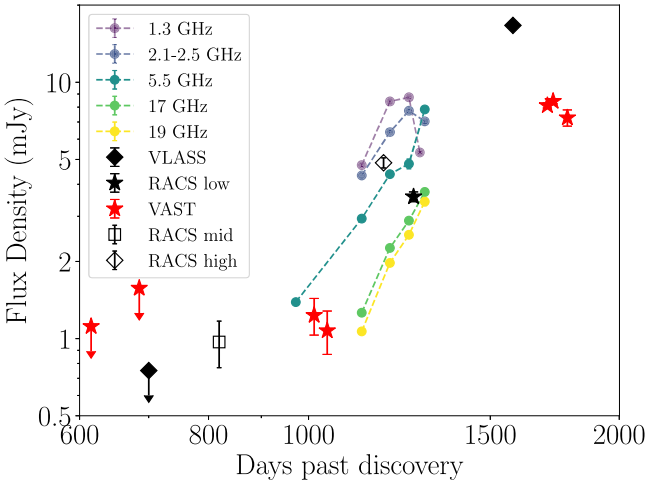

Figure 4. Light curve of TDE AT 2018hyz using RACS/VAST data, VLASS data, and archival data (from Cendes et al. 2022). The archival light curve, at five different frequencies from 1.3 to 19 GHz, adapted from Cendes et al. (2022), is shown as multicolored dots for reference.

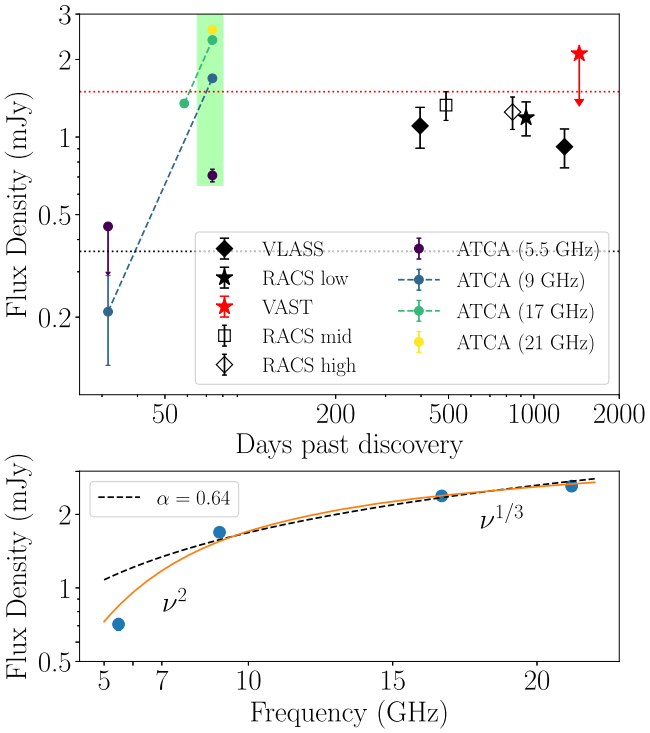

Figure 5. Top panel: light curve of the TDE AT 2019qiz using RACS, VLASS, and archival data at four different frequencies from 5.5 to 21 GHz from O'Brien et al. (2019a, 2019b). The green stripe shows the multifrequency epoch at $\sim$75 days, which we use for spectral fitting. The black dotted line shows the 3σ predisruption limit from VLASS data and the red dotted line shows the same from RACS-low epoch 1 data. Bottom panel: spectrum of this transient using observations at four different frequencies taken at the same epoch ($\sim$75 days post optical discovery; indicated by the box in the top panel). The orange line is the best-fit broken power law to the observed spectrum (see Section 3.5). The dashed black line is the best-fit single power-law spectrum (with spectral index $\alpha = 0.64$).

was <30% of the mean (see Figure 5). We also inspected the VLASS epoch 1 image that predated the optical disruption time and did not find a detection, putting a 3σ upper limit of 0.36 mJy on the persistent emission at 3 GHz. However, the transient rose to persistent levels of 1 mJy in the latter VLASS epochs (see Figure 5).

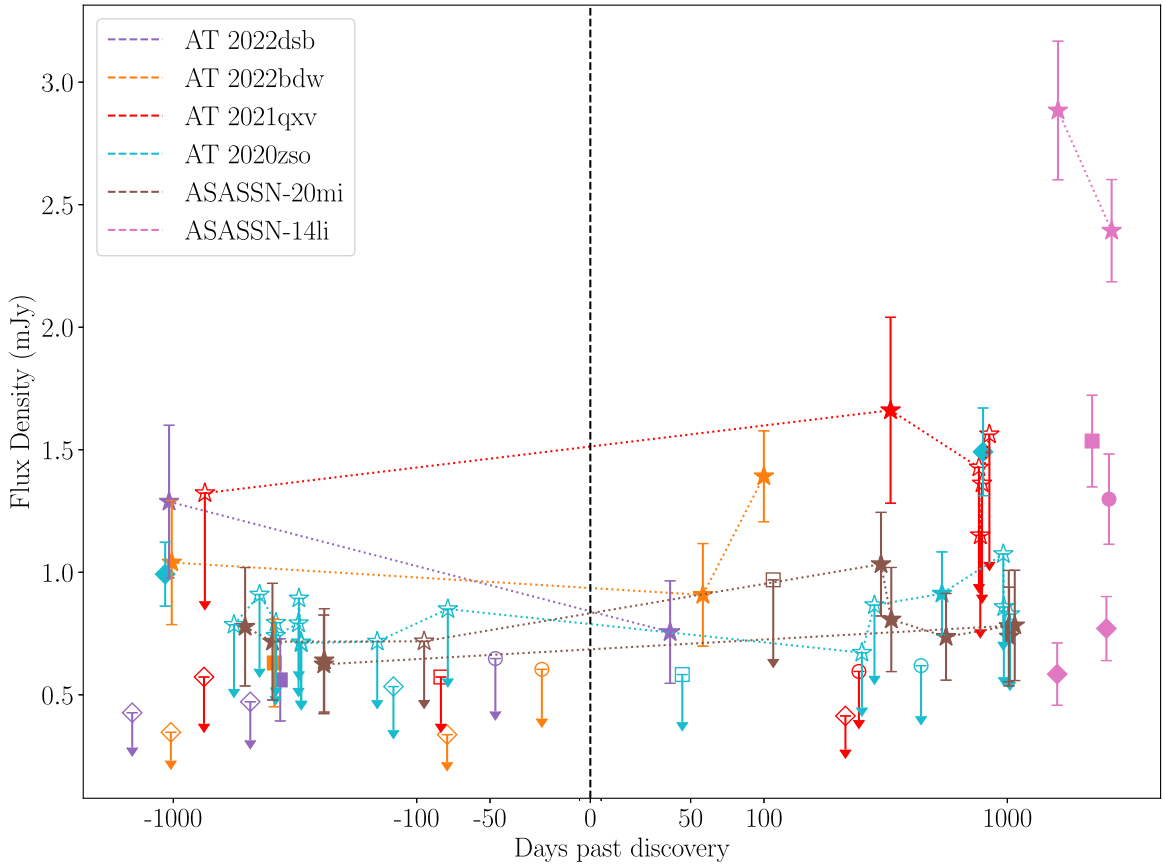

Figure 6. Light curves of the TDEs that did not show clear variability over the span of the RACS observations (roughly 3 yr) and might be contaminated by host emission: AT 2022dsb (purple), AT 2022bdw (orange), AT 2021qxv (red), AT 2020zso (cyan), ASASSN-20mi (brown), and ASASSN-14li (magenta). For each TDE the RACS-low data are shown as stars, RACS-mid data as squares, RACS-high data as circles, and the VLASS data as diamonds. Filled markers represent detections and open markers represent upper limits. The black dashed line shows the optical outburst time. Where possible, we use RACS+VLASS measurements to estimate the slope of the power-law spectrum (see Section 3.6).

Motivated by this behavior, we wanted to see whether the early-time behavior was consistent with an afterglow or whether it was different, in which case it might provide clues to the nature of the underlying emission. Using the data from O'Brien et al. (2019a, 2019b), we found that the initial rise time estimated at different frequencies seems to be consistent with $t^{2.5}$ at both 17 and 9 GHz. This $t^{2.5}$ increase was also consistent with the nondetection of this transient at 5.5 GHz at early times. The spectrum at $\sim$75 days seemed to be inconsistent with an SSA spectrum ($S_\nu \propto \nu^{5/2}$), so we tried to model the break frequency as a minimal frequency (ν_m) instead of the self-absorption frequency (see spectrum 1 in Figure 1 of Granot & Sari 2002). Here the spectral indices of the two rising power laws are $+2$ (Rayleigh–Jeans tail) at frequencies below the break and $+1/3$ at frequencies above it. We found a reasonable fit to the spectrum in this case (see bottom panel of Figure 5) with the break frequency around $\sim$9 GHz. This is indicative that at early times the emission seems to be consistent with an afterglow.

We tried to reconcile with the late-time radio observations from RACS and VLASS. The lack of late-time evolution likely ruled out the scenario where the late-time activity was still dominated by the emission powered by the CNM interaction. It is also possible that there was prior nuclear activity (possibly from an AGN) in this galaxy, which is visible once the transient faded away. The nondetection in VLASS and RACS data before the optical discovery makes this unlikely, but it cannot be ruled out entirely.[26] Although not temporally simultaneous, if we assume that the source is persistent and nonvariable, the spectrum might be consistent with a flat spectrum at late times, using the RACS and VLASS data. It might be possible that a jet was launched at early times and we are looking directly into the emission from the jet at late times, which could explain the flat spectrum. If this were the case, then it might be an interesting situation in which late-time emission from the jet was directly seen and would add to the small sample of jetted radio TDEs, but given the sparsity of the data, this cannot be firmly established.

3.6. Steady Radio Sources: Probable AGN/Host Galaxy Emission

In addition to the candidates where a rising/declining behavior is clearly seen, there are cases where the light curve showed little variation or was consistent with a nonvarying source (the underlying host galaxy or AGN). An AGN may be intrinsically variable, or variable due to external effects such as scintillation (Jauncey et al. 2016). In both cases, if the flux density was consistent with a steady source within error bars between the two RACS epochs, we considered that to result from underlying AGN activity (clearly this is a conservative assumption, as we could be averaging over

[26] In particular, the variation in AGN flux density with respect to the VLASS nondetection in epoch 1 has to be at least a factor of $\sim$5–6.

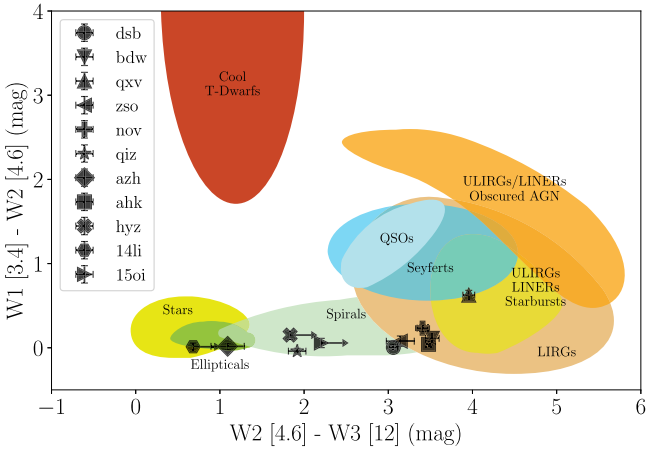

Figure 7. WISE color–color plot showing the magnitude difference in band 1 (W1) and band 2 (W2) on the *y*-axis, and band 2 (W2) and band 3 (W3) on the *x*-axis. The contours for different object classes are adopted from Wright et al. (2010). We used a W1 − W2 color of >0.8 to classify an object as an AGN.

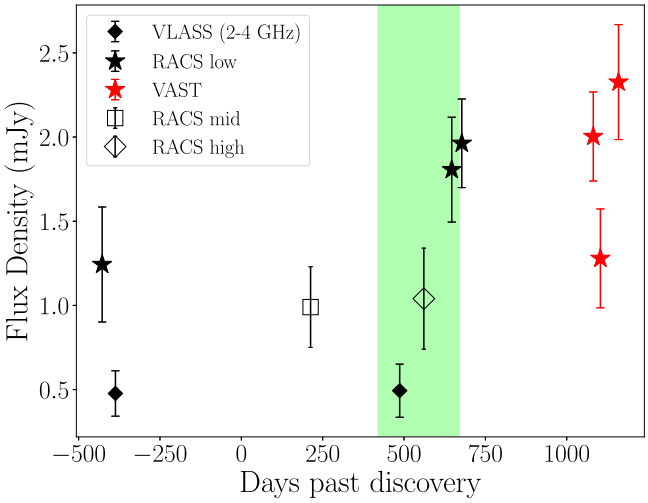

Figure 8. Light curve of TDE AT 2020nov using RACS, VAST, and VLASS data, all resulting in detections, with very little variability. The green stripe shows the data points used to measure the spectral index of the power-law spectrum.

peaks or declines given our sparse sampling). Below we note such examples (see Figure 6). We cross-matched the TDEs in our sample with the Wide-field Infrared Survey Explorer (WISE) catalog (Wright et al. 2010) to look for AGN signatures. Figure 7 shows the identified counterparts on a WISE color–color plot (Wright et al. 2010). We used a color difference of WISE band 1 (3.4 μm) − WISE band 2 (4.6 μm) > 0.8 (Wright et al. 2010) to classify an object as an AGN.

1. *AT 2020nov*: AT 2020nov was detected in both epochs of RACS-low with no significant evolution between them, and also in RACS-mid and RACS-high (see Figure 8). The first RACS-low observation predated the optical outburst by ∼400 days. We looked at the VLASS images and found that the same behavior was replicated at 3 GHz. Recently, Cendes et al. (2024) also reported AT 2020nov as probably dominated by an AGN in their study, with a nonevolving light curve at 6 GHz. The lack of variability in the observed data seems to indicate that the radio emission is likely coming from the AGN activity itself. Exploiting the nonvariability of this at different frequencies, we estimated the spectral index (see Figure 8), assuming a power-law spectrum $S_\nu \propto \nu^{-\alpha}$ for AGN activity. We used the data from RACS, VLASS, and Cendes et al. (2024) to find $\alpha = -0.64 \pm 0.04$, consistent with the typical AGN spectrum (Condon et al. 2002; Sabater et al. 2019).
2. *AT 2022dsb*: AT 2022dsb was discovered by Stanek & Kochanek (2022) on 2022 March 1 and had a radio detection reported by Goodwin et al. (2022a) roughly 20 days later, but the transient nature of this source was not confirmed. RACS-low epoch 1 had a 4σ prediscovery measurement that points to an underlying AGN or host galaxy emission, a conclusion strengthened by the detection in epoch 2, which showed little variability roughly 60 days after the optical outburst.[27] There was also a prediscovery measurement in RACS-mid. RACS-high and VLASS data resulted in upper limits (3σ; 0.6 mJy and 0.36 mJy respectively). Based on these detections and upper limits, we estimated the spectral index to be $\alpha = -0.7 \pm 0.3$, typical of AGNs.
3. *AT 2022bdw* (Tonry et al. 2022): No radio detection from this source has been reported so far, but we found prediscovery detections in RACS-low epoch 1 and RACS-mid data. Comparing these with RACS-low epoch 2, which was post optical outburst, we found that the flux density level was consistent with a nonvarying source, either the host AGN or host galaxy emission.[28] No emission was found in RACS-high or VLASS data, and using these we estimate the spectral index of the background emission to be $\alpha = -0.8 \pm 0.3$, again typical of AGNs.
4. *AT 2021qxv*: AT 2021qxv (Jones et al. 2021) was observed as a part of the VAST survey in addition to the RACS survey. However, no strong detection has been found in any of the RACS/VAST data except for detection in RACS-low epoch 2. RACS-mid showed a weak 3σ detection at this location, with RACS-high, VLASS, and Faint Images of the Radio Sky at Twenty-Centimeters (FIRST) data resulting in null detections, and hence we conclude that the RACS-low epoch 2 detection that we see is probably coming from an underlying AGN with a spectral index steeper than $\alpha = -1.1$.[29]
5. *AT 2020zso*: Discovered by Forster et al. (2020), very weak radio detection of 22 ± 7 μJy at 15 GHz was reported roughly one month later by Alexander et al. (2021), but following this, a null detection was made with the uGMRT (Roy et al. 2021) at the central frequencies of 0.65 and 1.26 GHz (upper limits of 46.6 and 51.2 μJy). No strong detections were made in RACS/VAST data except for a single detection in RACS-low epoch 2. VLASS data contain a 5σ detection in epoch 3.1, but the VAST observation that succeeded this resulted in nondetections, so we cannot conclusively establish any

[27] There is a WISE counterpart within 1″ of this position, but the WISE colors were not sufficiently conclusive to claim an AGN.

[28] This was one of the few fields that was observed twice as a part of RACS-low epoch 2, separated by 45 days, and the flux density was consistent with a nonvarying source to within 2σ.

[29] WISE colors point to a probable AGN.

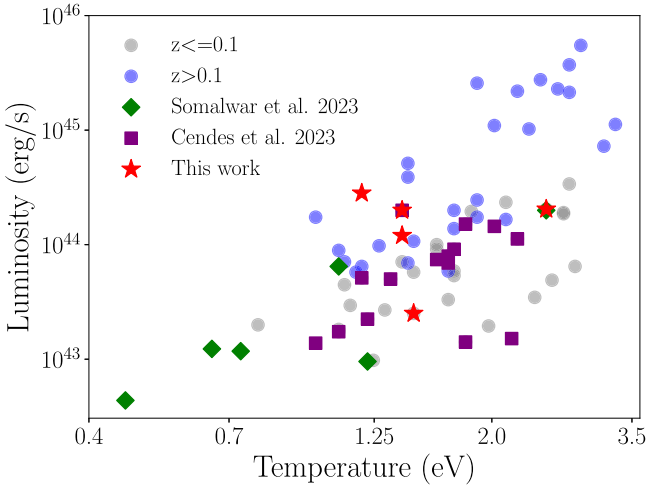

Figure 9. Blackbody luminosity vs. temperature of the nonrelativistic TDEs detected by various surveys. The background gray circles show the optical sample from the ZTF (Hammerstein et al. 2023; Yao et al. 2023) that are within a redshift of $z = 0.1$ and the blue circles show the TDE sample with $z > 0.1$. The red stars show the optically discovered TDEs that are detected in our radio sample. The purple squares show the optically discovered TDEs that resulted in radio detections in a targeted follow-up study by Cendes et al. (2024). The green diamonds show the TDEs that are independently identified in radio by Somalwar et al. (2023), but then confirmed optically. Where multiple points overlap, sources are common to multiple samples.

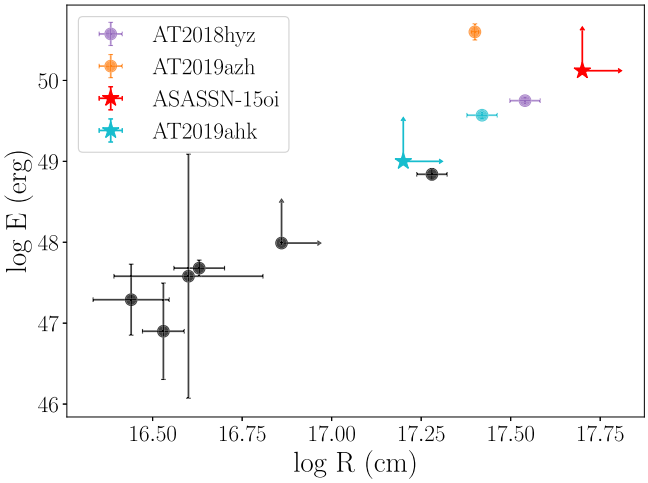

Figure 10. Estimates of equipartition radius and minimum total energy of the system, where possible, for the TDEs in our sample and archival TDEs (taken from Cendes et al. 2024). For our sample of TDEs, estimates derived from this study are shown as stars and those from the archival studies (Horesh et al. 2021; Cendes et al. 2022; Christy et al. 2024) are shown as colored circles. Estimates for archival TDEs that show late-time activity are shown as black dots (adapted from Cendes et al. 2024).

late-time transient activity from this source. It might be possible that the transient might take longer to rise at lower frequencies (Chevalier 1998), in which case future data from the VAST full survey will be very useful to check this. However, with the current data, we cannot rule out AGN variability.

6. *ASASSN-14li*: ASASSN-14li (Jose et al. 2014; Alexander et al. 2016; Holoien et al. 2016) showed late-time fading that continued until ∼600 days in some bands (Bright et al. 2018). We found radio detections at this position in both RACS-low epochs, but consistent with a steady flux density level. This source was also detected in RACS-mid, RACS-high, and VLASS, with no sign of evolution in the last of these. Comparing the archival FIRST measurement of 2.68 ± 0.15 mJy at 1.4 GHz with the RACS-mid observations indicates a ∼40% decrease in the flux density, indicating that the transient possibly faded away and we are looking at the variability from an AGN. Using RACS and VLASS data, we find the spectral index $\alpha = -0.95 \pm 0.14$.

4. Discussion

4.1. On the Nature of Detections

Understanding the sample biases in all-sky searches is important in estimating the rates and expectations for future surveys. In particular, understanding whether our radio-detected sample of TDEs forms an unbiased representation of the underlying optical population becomes important for future projections. Figure 9 shows the optical properties of the TDEs (blackbody luminosity versus temperature, as estimated from the optical data) that resulted in radio detections in the RACS-low survey. Comparing the radio detections in optically discovered TDEs using the sample for this study and that from Cendes et al. (2024), we do not see preferential occupation of radio-detected TDEs in this phase space. We do see that there are no radio detections of TDEs with both high temperatures and high luminosities (top right corner of the plot), but that can be attributed to the redshift because we do not expect detectable radio emission (given the current sensitivity limits of surveys like RACS/VLASS) from that subpopulation.[30] In the subsample of optical TDEs from which radio emission can be detected ($z \lesssim 0.1$), our sample, as well as the sample from Cendes et al. (2024), is not biased toward certain classes of optical TDEs, which suggests that the late-time detection of radio emission in TDEs might not be coming from a particular population of TDEs, but is a common feature of subrelativistic TDEs in general. We then compare our estimates of the emission radius and minimum energy injected into the outflow with archival studies, under the equipartition situation (see Figure 10). We caution the reader that a strict comparison would need accurate modeling of the expansion properties of the outflow (linear/accelerating/decelerating) to compare estimates from different times. We hence restrict the sample to those TDEs that show late-time radio emission. Using the samples from Horesh et al. (2021), Cendes et al. (2022, 2024), and Christy et al. (2024), we find that our estimates for the emission radius and the energy injected are consistent with those reported in the literature.

Somalwar et al. (2023) did an untargeted search for TDEs using the first two epochs of VLASS data, and independently discovered radio-first detections of optically bright TDEs. These are shown as the green scatter in Figure 9. While some of these seem to be consistent with the population of optically selected radio TDEs, Somalwar et al. (2023) suggest that some radio-discovered optically bright TDEs can have lower blackbody temperatures and luminosities, which can be partly due to TDEs occurring in dusty environments. Data from the RACS survey, but also more importantly from the VAST survey, which has a cadence of ∼2 months, should be very useful in conducting such untargeted searches.

[30] This is under the expectation of detecting radio emission from a subrelativistic outflow with $\nu L_\nu \approx 10^{38}$ erg s^{-1}.

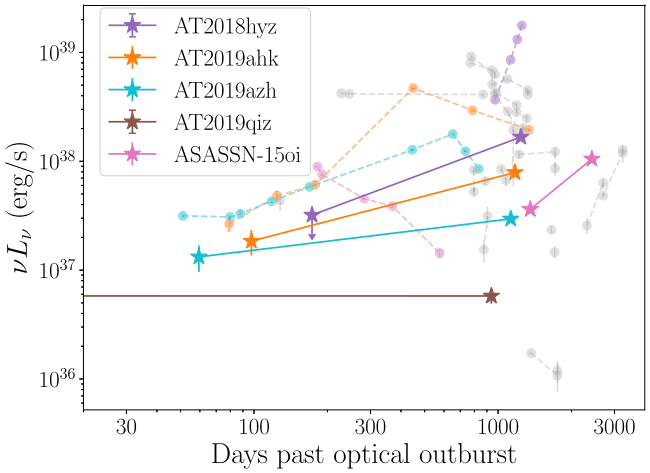

Figure 11. The radio luminosity of the five strong TDE detections in the RACS data set at 887.5 MHz. The solid line shows radio luminosity from RACS detections while the dashed lines show the same from 5–7 GHz (data adapted from Horesh et al. 2021; Cendes et al. 2022; Goodwin et al. 2022b; Christy et al. 2024). Shown in gray in the background are the light curves (at 6 GHz) of the archival TDEs detected by Cendes et al. (2024) and Alexander et al. (2020) from optically selected TDEs.

4.2. Projections for the VAST Survey

One of the important questions for an all-sky survey such as RACS is the detection efficiency. Figure 11 shows the radio luminosity at 887.5 MHz of the TDEs detected in the RACS survey compared to those of the population. We see that all of these detections have $\nu L_\nu \approx 10^{38}$ erg s^{-1}. We caution that comparison between light curves from our sample at 887.5 MHz and archival light curves at 6 GHz can be nontrivial and that the inferred radio luminosity νL_ν can have frequency dependence if L_ν does not exactly scale as ν^{-1}. Thus, if the spectral index is steeper than -1, the radio luminosity estimated from RACS will be an overestimation for the population (in Figure 11), and if shallower than -1, it will be an underestimation. Despite this, if we assume $\nu L_\nu \approx 10^{38}$ erg s^{-1} to be a typical estimate at 887.5 MHz, then given the sensitivity of the RACS survey (rms noise of 0.25 mJy beam^{-1}), it should be complete out to $z = 0.075$ ($d_L = 350$ Mpc).

We then look at the total population of potentially detectable TDEs. We require that they (i) are in the RACS footprint ($<41^\circ$ decl.), (ii) occurred before the RACS-low epoch 2 (2022 April), and (iii) are within $z = 0.075$, which results in 23 TDEs. Out of these, we detect five candidates where we are most likely seeing the afterglow and as many as six other events where we might be seeing the host AGN. Counting the five detections yields a (90% confidence; estimated using Gehrels 1986) detection rate of 22^{+15}_{-11}%. This is slightly more than but consistent within errors with Alexander et al. (2020), but slightly less than Cendes et al. (2024), who find late-time radio activity in as many as 40% of optically selected TDEs. It is worth mentioning here that, unlike a targeted search (e.g., Cendes et al. 2024), where continuous monitoring is done after initial detection, our results are based on observations roughly separated by 3 yr and hence we are completely insensitive to TDEs that rose and declined within this period, or to some of the most recent TDEs (that happened within a year of RACS-low epoch 2), which are still rising, but are currently below our sensitivity threshold. Hence this detection efficiency can be considered as a conservative lower limit for future efforts: a survey with a longer duration and finer time sampling would be able to detect more sources at the same sensitivity threshold.

Recently Cendes et al. (2024) performed a comprehensive late-time follow-up of a sample of 23 TDEs and found radio emission lasting on timescales of about a year in roughly 50% of the TDEs. Using the first 3 yr of optical data from ZTF, Yao et al. (2023) constrained the volumetric rate of optical TDEs to be $3.1^{+0.6}_{-1.0} \times 10^{-7}$ Mpc^{-3} yr^{-1}. If we assume that as many as 50% of optical TDEs (following Cendes et al. 2024) are capable of producing detectable late-time radio emission, then the current constraints on the rate of optical TDEs imply a rate of 1.5×10^{-7} Mpc^{-3} yr^{-1} for optically selected, radio-emitting TDEs. This rate, coupled with the sensitivity of the VAST survey (rms noise of 0.25 mJy beam^{-1}), its footprint (roughly a quarter of the total sky), and the survey lifetime (4 yr), implies that VAST should be able to detect $\sim$20 optically selected radio TDEs over the full survey. TDEs can also occur in highly dust-obscured environments, in which emission can be better studied at lower frequencies such as the infrared, where the emission can be powered by dust echoes (van Velzen et al. 2016, 2021; Jiang et al. 2021b), and radio wavelengths, which need ambient material for the outflows/jets to interact with. The rate of the radio-bright optically quiet TDEs is highly uncertain currently, particularly due to the lack of such studies. Hence the abovementioned sample of $\sim$20 TDEs can only be considered a lower limit on the detectable sample, given the current optical rate.

4.3. RACS/VAST as a Sub-GHz Reference Map

Radio emission from TDEs can last years, and hence obtaining a robust host spectrum in the absence of one might imply that we need to wait for years before the transient fades away and the host galaxy dominates again. RACS, and in particular VAST, can be tremendously helpful in this respect since it provides a low-frequency (where the emission is brighter) reference image, that can be used to study the long-term variability (or lack thereof) of the host galaxy pre-explosion. To illustrate this, we provide the example of AT 2023clx, where we can look for the pre-explosion radio emission using RACS data.

AT 2023clx was discovered by Stanek (2023) on 2023 February 22, well after RACS-low epoch 2. A radio detection was reported four days later by Sfaradi et al. (2023) consistent with the position of the optical transient. We found a persistent source in both epochs of RACS-low data at the optical location and, using nondetections in VLASS, we constrain the radio spectrum of the host to be steeper than -1.35. For future observing campaigns that aim to do dedicated follow-up of these TDEs, RACS data can be very useful in estimating the level of host contamination. With the availability of VAST full survey data, not only can radio-first discoveries be made, but also a well-sampled light curve with a cadence of 2 months leading up to the optical outburst can be obtained.

5. Conclusions

We conducted an untargeted search for radio emission in optically selected TDEs using data from the RACS survey, which resulted in five TDEs where the light curve showed significant evolution. For each of these TDEs, we modeled the

evolution to show that the radio evolution at late times can undergo rebrightening and can be complex. We found that late-time activity can be quite common at radio wavelengths in subrelativistic TDEs, adding to the sample presented by Cendes et al. (2024), who reached similar conclusions from targeted searches. Our search was based on the variability of the source over a timescale of roughly 3 yr, which makes us insensitive to TDEs that evolve on timescales shorter than this, and we estimate the rate of optical TDEs in which late-time radio emission can be observed to be $22^{+15}_{-11}\%$. Using the current optical rates, we estimate a conservative lower limit on the number of TDEs that can be detected in the VAST survey to be $\sim$20 over its survey span (4 yr).

Acknowledgments

We thank an anonymous referee for helpful comments. A.A. and D.L.K. are supported by NSF grant AST-1816492. Parts of this research were conducted by the Australian Research Council Centre of Excellence for Gravitational Wave Discovery (OzGrav), project number CE170100004. The Dunlap Institute is funded through an endowment established by the David Dunlap family and the University of Toronto. A.H. is grateful for the support by the the United States–Israel Binational Science Foundation (BSF grant 2020203) and by the Sir Zelman Cowen Universities Fund. This research was supported by the Israel Science Foundation (grant No. 1679/23). H.D. acknowledges support from the Walter C. Sumner Memorial Fellowship and the Natural Sciences and Engineering Research Council of Canada (NSERC) through a Postgraduate Scholarship. J.P. is supported by Australian Government Research Training Program Scholarships. K.R. thanks the LSST-DA Data Science Fellowship Program, which is funded by LSST-DA, the Brinson Foundation, and the Moore Foundation; G.R.S. is supported by NSERC Discovery grant No. RGPIN-2021-0400. This scientific work uses data obtained from Inyarrimanha Ilgari Bundara/the Murchison Radio-astronomy Observatory. The Australian SKA Pathfinder is part of the Australia Telescope National Facility (https://ror.org/05qajvd42), which is managed by CSIRO. Operation of ASKAP is funded by the Australian Government with support from the National Collaborative Research Infrastructure Strategy. ASKAP uses the resources of the Pawsey Supercomputing Centre. The establishment of ASKAP, the Murchison Radio-astronomy Observatory, and the Pawsey Supercomputing Centre are initiatives of the Australian Government, with support from the Government of Western Australia and the Science and Industry Endowment Fund.

Facility: ASKAP.

Appendix

Below we provide the radio flux density measurements (RACS and VLASS data) for TDEs detected in RACS survey in Table A1 and upper limits (RACS) for nondetections in Table A2.

Table A1
Radio Properties of the TDEs Found in the RACS-low Data Set

Name	R.A.	Decl.	Discovery (UT)	z	δt (days)	RACS-low (mJy)	RACS-mid (mJy)	RACS-high (mJy)	VLASS (mJy)
ASASSN-15oi	2015-08-14	$20^h39^m09\overset{s}{.}1$	$-30^d45^m21^s$	0.02	1355.1	4.21 ± 0.27	⋯	⋯	⋯
				⋯	1417.3	⋯	⋯	⋯	8.95 ± 1.35
				⋯	1961.3	⋯	10.52 ± 0.19	⋯	⋯
				⋯	2350.2	⋯	⋯	7.45 ± 0.2	⋯
				⋯	2377.7	⋯	⋯	⋯	4.95 ± 0.76
				⋯	2424.0	12.2 ± 0.15	⋯	⋯	⋯
				⋯	2860.9	7.28 ± 0.17	⋯	⋯	⋯
				⋯	2882.8	7.42 ± 0.27	⋯	⋯	⋯
				⋯	2938.6	6.51 ± 0.2	⋯	⋯	⋯
AT 2019ahk	2019-01-29T21:50:24	$07^h00^m11\overset{s}{.}5$	$-66^d02^m24^s$	0.026	97.5	1.24 ± 0.33	⋯	⋯	⋯
				⋯	738.6	⋯	4.69 ± 0.21	⋯	⋯
				⋯	1090.7	⋯	⋯	6.4 ± 0.2	⋯
				⋯	1172.5	5.87 ± 0.29	⋯	⋯	⋯
AT 2019azh	2019-02-22T00:28:48	$08^h13^m16\overset{s}{.}9$	$22^d38^m54^s$	0.022	51.9	⋯	⋯	⋯	<0.58
				⋯	59.4	1.27 ± 0.35	⋯	⋯	⋯
				⋯	682.7	⋯	3.88 ± 0.19	⋯	⋯
				⋯	1025.3	⋯	⋯	⋯	1.22 ± 0.22
				⋯	1039.8	⋯	⋯	2.38 ± 0.21	⋯
				⋯	1127.5	2.83 ± 0.2	⋯	⋯	⋯
AT 2018hyz	2018-11-06T15:21:36	$10^h06^m50\overset{s}{.}9$	$01^d41^m34^s$	0.046	−304.2	⋯	⋯	⋯	<0.39
				⋯	172.9	<0.69	⋯	⋯	⋯
				⋯	294.4	<0.78	⋯	⋯	⋯
				⋯	357.2	<0.81	⋯	⋯	⋯
				⋯	358.2	<0.75	⋯	⋯	⋯
				⋯	408.2	<0.73	⋯	⋯	⋯
				⋯	430.1	<0.75	⋯	⋯	⋯
				⋯	431.1	<0.85	⋯	⋯	⋯
				⋯	436.1	<0.82	⋯	⋯	⋯
				⋯	437.1	<0.68	⋯	⋯	⋯
				⋯	438.1	<0.61	⋯	⋯	⋯
				⋯	591.7	<0.67	⋯	⋯	⋯
				⋯	661.5	<0.94	⋯	⋯	⋯
				⋯	676.2	⋯	⋯	⋯	0.54 ± 0.17
				⋯	795.2	⋯	0.96 ± 0.21	⋯	⋯
				⋯	988.6	1.23 ± 0.2	⋯	⋯	⋯
				⋯	1018.5	1.07 ± 0.21	⋯	⋯	⋯
				⋯	1158.2	⋯	⋯	4.85 ± 0.22	⋯
				⋯	1240.0	3.58 ± 0.16	⋯	⋯	⋯
				⋯	1553.8	⋯	⋯	⋯	16.67 ± 2.5
				⋯	1679.8	8.12 ± 0.18	⋯	⋯	⋯
				⋯	1701.7	8.43 ± 0.19	⋯	⋯	⋯
				⋯	1757.5	7.27 ± 0.53	⋯	⋯	⋯
AT 2019qiz	2019-09-19T11:59:43	$04^h46^m37\overset{s}{.}9$	$-10^d13^m35^s$	0.015	−617.3	⋯	⋯	⋯	<0.36
				⋯	−142.2	<1.55	⋯	⋯	⋯
				⋯	396.9	⋯	⋯	⋯	1.1 ± 0.26
				⋯	490.0	⋯	1.33 ± 0.17	⋯	⋯
				⋯	841.1	⋯	⋯	1.25 ± 0.18	⋯
				⋯	938.8	1.19 ± 0.18	⋯	⋯	⋯
				⋯	1282.5	⋯	⋯	⋯	0.92 ± 0.21
				⋯	1387.6	<9.31	⋯	⋯	⋯
				⋯	1445.4	<2.11	⋯	⋯	⋯
AT 2020zso	2020-11-12T03:36:05.003	$22^h22^m17\overset{s}{.}1$	$-07^d16^m00^s$	0.061	−1080.0	⋯	⋯	⋯	0.99 ± 0.2
				⋯	−563.2	<0.79	⋯	⋯	⋯
				⋯	−442.4	<0.91	⋯	⋯	⋯
				⋯	−379.6	<0.74	⋯	⋯	⋯
				⋯	−378.7	<0.79	⋯	⋯	⋯
				⋯	−305.9	<0.79	⋯	⋯	⋯
				⋯	−304.9	<0.89	⋯	⋯	⋯
				⋯	−298.8	<0.71	⋯	⋯	⋯
				⋯	−297.8	<0.71	⋯	⋯	⋯
				⋯	−145.3	<0.72	⋯	⋯	⋯
				⋯	−124.6	⋯	⋯	⋯	<0.54
				⋯	−74.5	<0.85	⋯	⋯	⋯

Table A1
(Continued)

Name	R.A.	Decl.	Discovery (UT)	z	δt (days)	RACS-low (mJy)	RACS-mid (mJy)	RACS-high (mJy)	VLASS (mJy)
				⋯	46.2	⋯	<0.58	⋯	⋯
				⋯	252.7	<0.67	⋯	⋯	⋯
				⋯	284.5	<0.87	⋯	⋯	⋯
				⋯	442.1	⋯	⋯	<0.62	⋯
				⋯	538.8	0.91 ± 0.17	⋯	⋯	⋯
				⋯	794.8	⋯	⋯	⋯	1.49 ± 0.29
				⋯	962.7	<1.07	⋯	⋯	⋯
				⋯	967.7	<0.86	⋯	⋯	⋯
				⋯	1025.6	<0.83	⋯	⋯	⋯
AT 2021qxv	2021-05-10T10:50:52.800	$15^h18^m59\overset{s}{.}3$	$-03^d11^m45^s$	0.183	−748.0	⋯	⋯	⋯	<0.59
				⋯	−741.9	<1.32	⋯	⋯	⋯
				⋯	−79.5	⋯	<0.57	⋯	⋯
				⋯	216.2	⋯	⋯	⋯	<0.41
				⋯	245.6	⋯	⋯	<0.6	⋯
				⋯	331.3	1.66 ± 0.38	⋯	⋯	⋯
				⋯	764.2	<1.43	⋯	⋯	⋯
				⋯	774.1	<1.15	⋯	⋯	⋯
				⋯	787.1	<1.36	⋯	⋯	⋯
				⋯	843.9	<1.56	⋯	⋯	⋯
AT 2022bdw	2022-01-31T09:37:26.400	$08^h25^m10\overset{s}{.}4$	$18^d34^m57^s$	0.038	−1023.4	⋯	⋯	⋯	<0.36
				⋯	−1014.9	1.04 ± 0.25	⋯	⋯	⋯
				⋯	−384.7	⋯	0.63 ± 0.18	⋯	⋯
				⋯	−75.0	⋯	⋯	⋯	<0.35
				⋯	−30.6	⋯	⋯	<0.6	⋯
				⋯	56.1	0.91 ± 0.21	⋯	⋯	⋯
				⋯	100.0	1.39 ± 0.19	⋯	⋯	⋯
AT 2022dsb	2022-03-01T13:40:47	$15^h42^m21\overset{s}{.}7$	$-22^d40^m14^s$	0.023	−1475.1	⋯	⋯	⋯	<0.46
				⋯	−1041.0	1.29 ± 0.3	⋯	⋯	⋯
				⋯	−482.8	⋯	⋯	⋯	<0.48
				⋯	−363.7	⋯	0.56 ± 0.16	⋯	⋯
				⋯	−47.5	⋯	⋯	<0.65	⋯
				⋯	41.2	0.76 ± 0.21	⋯	⋯	⋯
ASASSN-14li	2014-11-22T00:00:00	$12^h48^m15\overset{s}{.}2$	$17^d46^m26^s$	0.021	1602.4	⋯	⋯	⋯	0.58 ± 0.15
				⋯	1614.5	2.88 ± 0.28	⋯	⋯	⋯
				⋯	2230.0	⋯	1.54 ± 0.19	⋯	⋯
				⋯	2552.5	⋯	⋯	⋯	0.77 ± 0.17
				⋯	2615.9	⋯	⋯	1.3 ± 0.18	⋯
				⋯	2681.7	2.39 ± 0.2	⋯	⋯	⋯

(This table is available in machine-readable form in the online article.)

Table A2
Upper Limits (3σ) on the Radio Emission from the RACS/VAST Survey for the Sample of TDEs That Are in the RACS Footprint but Resulted in Nondetections

Name	δt	Flux Limit		Luminosity Limit[a]	
		RACS	VAST	RACS	VAST
	(days)	(mJy)	(mJy)	(erg s^{-1})	(erg s^{-1})
AT 2016fnl	1121	0.8	⋯	4.6×10^{36}	⋯
AT 2016fnl	2047	0.6	⋯	3.5×10^{36}	⋯
AT 2018dyb	466	2.1	⋯	1.5×10^{37}	⋯
AT 2018dyb	1370	2.4	⋯	1.6×10^{37}	⋯
AT 2018fyk	419	0.6	⋯	5.0×10^{37}	⋯
AT 2018fyk	517	⋯	0.7	⋯	5.4×10^{37}
AT 2018fyk	518	⋯	0.5	⋯	4.4×10^{37}
AT 2018fyk	520	⋯	0.5	⋯	4.2×10^{37}
AT 2018fyk	521	⋯	0.5	⋯	4.3×10^{37}
AT 2018fyk	727	⋯	0.6	⋯	4.9×10^{37}
AT 2018fyk	1024	⋯	0.5	⋯	3.8×10^{37}
AT 2018fyk	1049	⋯	0.4	⋯	3.7×10^{37}
AT 2018fyk	1080	⋯	0.5	⋯	3.7×10^{37}
AT 2018fyk	1334	0.4	⋯	3.3×10^{37}	⋯
AT 2018fyk	1762	⋯	0.7	⋯	5.4×10^{37}
AT 2018fyk	1763	⋯	0.5	⋯	3.9×10^{37}
AT 2018hco	355	1.1	⋯	2.2×10^{38}	⋯
AT 2018hco	1282	0.9	⋯	1.6×10^{38}	⋯
AT 2018iih	320	0.7	⋯	9.1×10^{38}	⋯
AT 2018iih	1241	0.5	⋯	6.2×10^{38}	⋯
AT 2018lna	271	0.8	⋯	1.6×10^{38}	⋯
AT 2018lna	1193	0.6	⋯	1.2×10^{38}	⋯
AT 2018zr	571	0.7	⋯	7.8×10^{37}	⋯
AT 2018zr	1491	0.6	⋯	6.5×10^{37}	⋯
AT 2019bhf	245	1.7	⋯	6.1×10^{38}	⋯
AT 2019bhf	1147	0.8	⋯	2.9×10^{38}	⋯
AT 2019dsg	191	0.9	⋯	5.6×10^{37}	⋯
AT 2019dsg	1095	0.6	⋯	3.6×10^{37}	⋯
AT 2019gte	139	0.8	⋯	1.5×10^{38}	⋯
AT 2019gte	252	⋯	0.8	⋯	1.5×10^{38}
AT 2019gte	252	⋯	1.0	⋯	1.7×10^{38}
AT 2019gte	254	⋯	1.0	⋯	1.8×10^{38}
AT 2019gte	255	⋯	0.7	⋯	1.2×10^{38}
AT 2019gte	255	⋯	0.9	⋯	1.5×10^{38}
AT 2019gte	462	⋯	0.8	⋯	1.4×10^{38}
AT 2019gte	760	⋯	0.6	⋯	1.1×10^{38}
AT 2019gte	783	⋯	0.7	⋯	1.1×10^{38}
AT 2019gte	814	⋯	0.7	⋯	1.2×10^{38}
AT 2019gte	1037	0.6	⋯	1.0×10^{38}	⋯
AT 2019gte	1484	⋯	0.6	⋯	1.1×10^{38}
AT 2019gte	1497	⋯	0.9	⋯	1.6×10^{38}
AT 2019lwu	86	0.8	⋯	2.8×10^{38}	⋯
AT 2019lwu	197	⋯	0.9	⋯	3.0×10^{38}
AT 2019lwu	198	⋯	0.9	⋯	2.9×10^{38}
AT 2019lwu	200	⋯	0.8	⋯	2.8×10^{38}
AT 2019lwu	200	⋯	0.9	⋯	3.0×10^{38}
AT 2019lwu	201	⋯	0.7	⋯	2.3×10^{38}
AT 2019lwu	201	⋯	0.7	⋯	2.5×10^{38}
AT 2019lwu	407	⋯	0.9	⋯	3.0×10^{38}
AT 2019lwu	706	⋯	0.8	⋯	2.7×10^{38}
AT 2019lwu	730	⋯	0.8	⋯	2.7×10^{38}
AT 2019lwu	760	⋯	0.7	⋯	2.5×10^{38}
AT 2019lwu	1001	0.6	⋯	1.9×10^{38}	⋯
AT 2019lwu	1444	⋯	0.7	⋯	2.5×10^{38}
AT 2019lwu	1444	⋯	0.8	⋯	2.7×10^{38}
AT 2019vcb	−52	0.8	⋯	1.4×10^{38}	⋯
AT 2019vcb	868	0.5	⋯	1.0×10^{38}	⋯
AT 2020acka	−421	3.3	⋯	1.2×10^{40}	⋯
AT 2020acka	479	1.3	⋯	4.5×10^{39}	⋯
AT 2020neh	−247	0.9	⋯	7.8×10^{37}	⋯
AT 2020neh	654	0.6	⋯	5.3×10^{37}	⋯
AT 2020pj	−79	0.6	⋯	6.4×10^{37}	⋯
AT 2020pj	822	0.5	⋯	5.2×10^{37}	⋯
AT 2020vwl	−361	0.7	⋯	2.0×10^{37}	⋯
AT 2020vwl	540	0.5	⋯	1.4×10^{37}	⋯
AT 2021ack	−455	1.1	⋯	4.7×10^{38}	⋯
AT 2021ack	447	1.0	⋯	4.5×10^{38}	⋯
AT 2021ack	484	0.8	⋯	3.7×10^{38}	⋯
AT 2021ack	885	⋯	1.1	⋯	5.1×10^{38}
AT 2021ack	905	⋯	1.3	⋯	5.8×10^{38}
AT 2021axu	−481	0.6	⋯	6.2×10^{38}	⋯
AT 2021axu	439	0.5	⋯	5.0×10^{38}	⋯
AT 2021blz	−472	0.7	⋯	3.3×10^{37}	⋯
AT 2021blz	445	0.5	⋯	2.4×10^{37}	⋯
AT 2021blz	886	⋯	0.5	⋯	2.3×10^{37}
AT 2021ehb	−487	0.8	⋯	5.3×10^{36}	⋯
AT 2021ehb	397	0.7	⋯	4.9×10^{36}	⋯
AT 2021gje	−504	1.0	⋯	4.3×10^{39}	⋯
AT 2021gje	380	0.6	⋯	2.5×10^{39}	⋯
AT 2021jjm	−540	1.3	⋯	7.8×10^{38}	⋯
AT 2021jjm	365	0.7	⋯	4.1×10^{38}	⋯
AT 2021jsg	−471	0.6	⋯	2.3×10^{38}	⋯
AT 2021jsg	449	0.5	⋯	2.0×10^{38}	⋯
AT 2021lo	−446	1.1	⋯	6.4×10^{38}	⋯
AT 2021lo	460	0.7	⋯	3.9×10^{38}	⋯
AT 2021lo	894	⋯	0.7	⋯	3.9×10^{38}
AT 2021lo	913	⋯	0.7	⋯	4.3×10^{38}
AT 2021mhg	−595	0.8	⋯	9.4×10^{37}	⋯
AT 2021mhg	331	0.6	⋯	7.4×10^{37}	⋯
AT 2021uqv	−674	0.8	⋯	2.2×10^{38}	⋯
AT 2021uqv	253	0.9	⋯	2.4×10^{38}	⋯
AT 2021uvz	−656	0.8	⋯	6.6×10^{38}	⋯
AT 2021uvz	265	0.6	⋯	5.2×10^{38}	⋯
AT 2021yte	−719	0.8	⋯	5.1×10^{37}	⋯
AT 2021yte	218	0.6	⋯	3.7×10^{37}	⋯
AT 2021yte	234	0.5	⋯	3.4×10^{37}	⋯
AT 2021yzv	−655	0.9	⋯	2.3×10^{39}	⋯
AT 2021yzv	228	0.8	⋯	2.0×10^{39}	⋯
AT 2022adm	−829	1.6	⋯	1.4×10^{38}	⋯
AT 2022adm	72	0.7	⋯	6.3×10^{37}	⋯
AT 2022arb	−833	1.0	⋯	8.7×10^{37}	⋯
AT 2022arb	−725	⋯	1.0	⋯	8.8×10^{37}
AT 2022arb	−721	⋯	1.1	⋯	9.6×10^{37}
AT 2022arb	−721	⋯	1.2	⋯	1.0×10^{38}
AT 2022arb	−720	⋯	0.9	⋯	8.1×10^{37}
AT 2022arb	−720	⋯	1.3	⋯	1.2×10^{38}
AT 2022arb	−719	⋯	4.0	⋯	3.5×10^{38}
AT 2022arb	−718	⋯	0.8	⋯	7.4×10^{37}
AT 2022arb	−718	⋯	1.2	⋯	1.1×10^{38}
AT 2022arb	−703	⋯	3.9	⋯	3.4×10^{38}
AT 2022arb	−512	⋯	3.8	⋯	3.4×10^{38}
AT 2022arb	−213	⋯	0.9	⋯	7.9×10^{37}
AT 2022arb	−190	⋯	0.7	⋯	6.5×10^{37}
AT 2022arb	−160	⋯	0.9	⋯	7.5×10^{37}
AT 2022arb	66	0.6	⋯	5.4×10^{37}	⋯
AT 2022arb	504	⋯	0.7	⋯	6.0×10^{37}
AT 2022arb	524	⋯	0.8	⋯	7.5×10^{37}
AT 2022czy	−843	0.9	⋯	2.7×10^{38}	⋯
AT 2022czy	39	0.7	⋯	1.9×10^{38}	⋯
AT 2022dyt	−885	0.7	⋯	8.3×10^{37}	⋯

Table A2
(Continued)

Name	δt	Flux Limit		Luminosity Limit[a]	
		RACS	VAST	RACS	VAST
	(days)	(mJy)	(mJy)	(erg s^{-1})	(erg s^{-1})
AT 2022dyt	33	0.6	⋯	7.0×10^{37}	⋯
AT 2022exr	−887	0.7	⋯	1.6×10^{38}	⋯
AT 2022exr	14	0.6	⋯	1.2×10^{38}	⋯

Note.
[a] Radio luminosity is estimated as νL_ν and we assume the emission to be spherical, which results in the inclusion of a 4π factor.

(This table is available in machine-readable form in the online article.)

ORCID iDs

Akash Anumarlapudi https://orcid.org/0000-0002-8935-9882
Dougal Dobie https://orcid.org/0000-0003-0699-7019
David L. Kaplan https://orcid.org/0000-0001-6295-2881
Tara Murphy https://orcid.org/0000-0002-2686-438X
Assaf Horesh https://orcid.org/0000-0002-5936-1156
Emil Lenc https://orcid.org/0000-0002-9994-1593
Laura Driessen https://orcid.org/0000-0002-4405-3273
Stefan W. Duchesne https://orcid.org/0000-0002-3846-0315
Hannah Dykaar https://orcid.org/0009-0008-6396-0849
B. M. Gaensler https://orcid.org/0000-0002-3382-9558
Timothy J. Galvin https://orcid.org/0000-0002-2801-766X
Joe Grundy https://orcid.org/0000-0002-4440-8046
George Heald https://orcid.org/0000-0002-2155-6054
Aidan W. Hotan https://orcid.org/0000-0001-7464-8801
Minh Huynh https://orcid.org/0000-0002-8314-9753
James K. Leung https://orcid.org/0000-0002-9415-3766
David McConnell https://orcid.org/0000-0002-2819-9977
Vanessa A. Moss https://orcid.org/0000-0002-3005-9738
Joshua Pritchard https://orcid.org/0000-0003-1575-5249
Kovi Rose https://orcid.org/0000-0002-7329-3209
Gregory Sivakoff https://orcid.org/0000-0001-6682-916X
Yuanming Wang https://orcid.org/0000-0003-0203-1196
Ziteng Wang https://orcid.org/0000-0002-2066-9823
Mark H. Wieringa https://orcid.org/0000-0002-7721-8660
Matthew T. Whiting https://orcid.org/0000-0003-1160-2077

References

Alexander, K. D., Berger, E., Guillochon, J., Zauderer, B. A., & Williams, P. K. G. 2016, ApJL, 819, L25
Alexander, K. D., van Velzen, S., Horesh, A., & Zauderer, B. A. 2020, SSRv, 216, 81
Alexander, K. D., Velzen, S. v., Miller-Jones, J., et al. 2021, ATel, 14337, 1
Anderson, M. M., Mooley, K. P., Hallinan, G., et al. 2020, ApJ, 903, 116
Andreoni, I., Coughlin, M. W., Perley, D. A., et al. 2022, Natur, 612, 430
Auchettl, K., Guillochon, J., & Ramirez-Ruiz, E. 2017, ApJ, 838, 149
Barniol Duran, R., Nakar, E., & Piran, T. 2013, ApJ, 772, 78
Bellm, E. C., Kulkarni, S. R., Graham, M. J., et al. 2019, PASP, 131, 018002
Bright, J. S., Fender, R. P., Motta, S. E., et al. 2018, MNRAS, 475, 4011
Cendes, Y., Berger, E., Alexander, K. D., et al. 2022, ApJ, 938, 28
Cendes, Y., Berger, E., Alexander, K. D., et al. 2024, ApJ, 971, 185
Chevalier, R. A. 1998, ApJ, 499, 810
Christy, C. T., Alexander, K. D., Cendes, Y., et al. 2024, arXiv:2404.12431
Condon, J. J., Cotton, W. D., & Broderick, J. J. 2002, AJ, 124, 675
Duchesne, S. W., Thomson, A. J. M., Pritchard, J., et al. 2023, PASA, 40, e034
Dykaar, H., Drout, M. R., Gaensler, B. M., et al. 2024, arXiv:2406.08371
Forster, F., Bauer, F. E., Munoz-Arancibia, A., et al. 2020, TNSTR, 2020-3449, 1
Gehrels, N. 1986, ApJ, 303, 336
Gezari, S. 2021, ARA&A, 59, 21
Goodwin, A., Anderson, G., Miller-Jones, J., et al. 2022a, ATel, 15293, 1
Goodwin, A. J., van Velzen, S., Miller-Jones, J. C. A., et al. 2022b, MNRAS, 511, 5328
Granot, J., & Sari, R. 2002, ApJ, 568, 820
Guzman, J., Whiting, M., Voronkov, M., et al., 2019 ASKAPsoft: ASKAP Science Data Processor Software, Astrophysics Source Code Library, ascl:1912.003
Hale, C. L., McConnell, D., Thomson, A. J. M., et al. 2021, PASA, 38, e058
Halpern, J. P., Gezari, S., & Komossa, S. 2004, ApJ, 604, 572
Hammerstein, E., van Velzen, S., Gezari, S., et al. 2023, ApJ, 942, 9
Holoien, T. W. S., Kochanek, C. S., Prieto, J. L., et al. 2016, MNRAS, 463, 3813
Holoien, T. W. S., Vallely, P. J., Auchettl, K., et al. 2019, ApJ, 883, 111
Horesh, A., Burger, N., Sfaradi, I., et al. 2022, ATel, 15307, 1
Horesh, A., Cenko, S. B., & Arcavi, I. 2021, NatAs, 5, 491
Hotan, A. W., Bunton, J. D., Chippendale, A. P., et al. 2021, PASA, 38, e009
Hung, T., Foley, R. J., Veilleux, S., et al. 2021, ApJ, 917, 9
Jauncey, D. L., Bignall, H. E., Kedziora-Chudczer, L., et al. 2016, Galax, 4, 62
Jiang, N., Liming, D., Wang, T., et al. 2016, ApJ, 828, L14
Jiang, N., Wang, T., & Dou, L. 2021a, ApJS, 252, 32
Jiang, N., Wang, T., Hu, X., et al. 2021b, ApJ, 911, 31
Jones, D. O., French, K. D., Agnello, A., et al. 2021, TNSTR, 2021-2199, 1
Jose, J., Guo, Z., Long, F., et al. 2014, ATel, 6777, 1
Krolik, J., Piran, T., Svirski, G., & Cheng, R. M. 2016, ApJ, 827, 127
Lacy, M., Baum, S. A., Chandler, C. J., et al. 2020, PASP, 132, 035001
Leung, J. K., Murphy, T., Lenc, E., et al. 2023, MNRAS, 523, 4029
Masterson, M., De, K., Panagiotou, C., et al. 2024, ApJ, 961, 211
Matsumoto, T., & Piran, T. 2023, MNRAS, 522, 4565
McConnell, D., Hale, C. L., Lenc, E., et al. 2020, PASA, 37, e048
Murphy, T., Chatterjee, S., Kaplan, D. L., et al. 2013, PASA, 30, e006
Murphy, T., Kaplan, D. L., Stewart, A. J., et al. 2021, PASA, 38, e054
Nakar, E., & Piran, T. 2011, Natur, 478, 82
Nicholl, M., Wevers, T., Oates, S. R., et al. 2020, MNRAS, 499, 482
O'Brien, A., Kaplan, D., Murphy, T., Yu, W., & Zhang, W. 2019a, ATel, 13310, 1
O'Brien, A., Kaplan, D., Murphy, T., Yu, W., & Zhang, W. 2019b, ATel, 13334, 1
Pacholczyk, A. G. 1970, Radio Astrophysics. Nonthermal Processes in Galactic and Extragalactic Sources (San Francisco, CA: Freeman)
Pasham, D. R., & van Velzen, S. 2018, ApJ, 856, 1
Patra, K. C., Lu, W., Brink, T. G., et al. 2022, MNRAS, 515, 138
Planck Collaboration, Aghanim, N., Akrami, Y., et al. 2020, A&A, 641, A6
Pritchard, J., Murphy, T., Heald, G., et al. 2024, MNRAS, 529, 1258
Ravi, V., Dykaar, H., Codd, J., et al. 2022, ApJ, 925, 220
Rees, M. J. 1988, Natur, 333, 523
Roy, R., Nayana, A. J., & Chandra, P. 2021, ATel, 14828, 1
Sabater, J., Best, P. N., Hardcastle, M. J., et al. 2019, A&A, 622, A17
Sfaradi, I., Beniamini, P., Horesh, A., et al. 2024, MNRAS, 527, 7672
Sfaradi, I., Horesh, A., Bright, J., et al. 2023, ATel, 15918, 1
Sfaradi, I., Horesh, A., Fender, R., et al. 2022, ApJ, 933, 176
Shappee, B. J., Prieto, J. L., Grupe, D., et al. 2014, ApJ, 788, 48
Siebert, M. R., Strasburger, E., Rojas-Bravo, C., & Foley, R. J. 2019, ATel, 13131, 1
Somalwar, J. J., Ravi, V., Dong, D. Z., et al. 2023, ApJ, 945, 142
Stanek, K. Z. 2023, TNSTR, 2023-421, 1
Stanek, K. Z., & Kochanek, C. S. 2022, TNSTR, 2022-559, 1
Tonry, J., Denneau, L., Weiland, H., et al. 2022, TNSTR, 2022-284, 1
van Velzen, S., Holoien, T. W. S., Onori, F., Hung, T., & Arcavi, I. 2020, SSRv, 216, 124
van Velzen, S., Mendez, A. J., Krolik, J. H., & Gorjian, V. 2016, ApJ, 829, 19
van Velzen, S., Pasham, D. R., Komossa, S., Yan, L., & Kara, E. A. 2021, SSRv, 217, 63
Wright, E. L., Eisenhardt, P. R. M., Mainzer, A. K., et al. 2010, AJ, 140, 1868
Yao, Y., Ravi, V., Gezari, S., et al. 2023, ApJL, 955, L6
Zauderer, B. A., Berger, E., Soderberg, A. M., et al. 2011, Natur, 476, 425